IEEE Access
Multidisciplinary | Rapid Review | Open Access Journal

Received July 25, 2019, accepted August 31, 2019, date of publication September 4, 2019, date of current version September 25, 2019.

Digital Object Identifier 10.1109/ACCESS.2019.2939383

Joint Symbol Timing and Channel Estimation for FBMC-OQAM Systems

LIMING LI[1], (Student Member, IEEE), LIQIN DING[1], (Member, IEEE), YANG WANG[1], PENG WU[1] (Student Member, IEEE), AND JILIANG ZHANG[2], (Senior Member, IEEE)

[1]School of Electronic and Information Engineering, Harbin Institute of Technology, Shenzhen 518055, China
[2]Department of Electronic and Electrical Engineering, The University of Sheffield, Sheffield S1 4ET, U.K.

Corresponding author: Yang Wang (yangw@hit.edu.cn)

This work was supported in part by the International Science and Technology Cooperation Program of China under Grant 2017YFE0118900, in part by the China Postdoctoral Science Foundation under Grant 2018M641829, and in part by the Science and Technology Project of Shenzhen under Grant JCYJ20170815140215733 and Grant JSGG20170822173002341.

ABSTRACT Filter bank multicarrier with offset quadrature amplitude modulation (FBMC-OQAM) can achieve very low out-of-band radiation and is considered to be an important candidate waveform for future communication networks. However, the synchronization sequence design and channel estimation issues are complicated in FBMC-OQAM systems owing to the pulses overlap and the intrinsic interference. In this paper, we propose a new training sequence pattern with a high bandwidth efficiency. A pilot symbol and two auxiliary data symbols are used to generate a conjugate symmetric sequence in the time domain while protecting the pilots from the intrinsic interference. Thus, channel estimation can be performed directly by the pilots, and an auto-correlation symbol timing algorithm is introduced by exploiting the conjugate symmetry property. In addition, a pulse tail truncation method is proposed to improve the bandwidth efficiency for burst-mode transmission. Finally, some numerical simulation results are presented to validate the proposed symbol timing, channel estimation, and truncation methods in various scenarios.

INDEX TERMS Channel estimation, FBMC-OQAM, signal detection, timing.

I. INTRODUCTION

In recent years, the filter bank multicarrier (FBMC) was proposed as an important candidate waveform technique to efficiently support the asynchronous and heterogeneous network scenarios expected in the future [1], e.g., massive machine-type communications (mMTC) [2] and cognitive radio (CR) [3]. Compared with orthogonal frequency division multiplexing (OFDM), which has been extensively used in many communication systems, such as long-term evolution (LTE), the FBMC employs pulse shaping to suppress the out-of-band (OOB) radiation [1]. Thus, FBMC systems can reduce the inter-carrier interference (ICI) and more flexibly utilize the spectrum than OFDM systems [4], [5].

One notable FBMC variant is the FBMC with offset quadrature amplitude modulation (FBMC-OQAM). Different from conventional OFDM that transmits complex-valued quadrature amplitude modulation (QAM) symbols at a given symbol rate, the FBMC-OQAM transmits real-valued pulse amplitude modulated (PAM) symbols at twice this symbol rate, with the orthogonality of the waveform restricted only to the real field [1]. With this type of modulation, the FBMC-OQAM achieves the highest spectral efficiency of an OFDM system without the cyclic prefix while the signal maintains good time-frequency localization (TFL) [1] [6].

Although the FBMC-OQAM has these merits, some signal processing issues are complicated owing to the pulse shaping and OQAM modulation, e.g., synchronization and channel estimation, which are two important issues for the performance of wireless communication systems [7], [8].

In FBMC-OQAM systems, multiple symbols overlap with each other in the time domain because of the long pulse tail; thus, the synchronization sequence design is not as straightforward as that for OFDM.

Synchronization methods for FBMC-OQAM systems, including both blind and data-aided schemes, have been investigated in the literature. Most blind schemes are dedicated to carrier frequency offset (CFO) estimation [9]–[11]. Based on the conjugate cyclostationarity property of FBMC-OQAM signals, a blind CFO estimation algorithm

The associate editor coordinating the review of this manuscript and approving it for publication was Kezhi Wang.

was proposed [9]. In addition to the conjugate cyclostationarity property, the unconjugate cyclostationarity property was also considered to further improve the CFO estimation performance in [10], [11].

For continuous-mode transmission, to address both the timing offset (TO) and CFO estimation, data-aided synchronization schemes are usually considered. A training sequence scheme with two identical parts was proposed in [12], and the training sequence was generated by transmitting a series of successive training data symbols to counteract the symbol overlapping effect. Because this scheme requires many training symbols, it decreases the bandwidth efficiency. As with most OFDM synchronization schemes, a constant-amplitude zero auto-correlation (CAZAC) sequence was considered for symbol timing in [13]. To construct a CAZAC sequence in the presence of pulse shaping and symbol overlapping effects, the value of the training data symbol must be calculated according to the preceding and following payload data symbol values. In [14], a method to generate a timing synchronization sequence with conjugate symmetry (CS) property applicable to continuous transmission was introduced; this sequence scheme only involves two symbols and thus maintains a very high bandwidth efficiency.

For burst mode-transmission, the start of the FBMC-OQAM signal approximately has CS property; a blind synchronization scheme was proposed in [15]. To further improve the synchronization performance, a data-aided preamble scheme that also used the CS property was investigated in [16]. A data preloading and truncation technique [17] was adopted to generate the preamble to increase the bandwidth efficiency. Recently, another synchronization sequence with a repeated conjugate symmetric (RCS) property was proposed in [18]. Both the preamble sequences with the CS property in [16] and [18] were generated with zero guard symbols to partly counteract the symbol overlapping effect.

Because the orthogonality only holds in the real field, the FBMC-OQAM signal suffers from imaginary intrinsic interference, and thus channel estimation can not be performed directly [22]. Guard symbols are usually employed to protect the pilots from the intrinsic interference in preamble-based channel estimation [19]–[21]. In the case of scattered-pilot patterns, an auxiliary pilot (AP) symbol can be used to mitigate the imaginary interference at each pilot position [22]. However, it turns out that the average power of the AP is boosted relative to that of payload data symbols. To avoid this energy waste, a precoding scheme was proposed in [23]. The neighboring symbols were linearly coded so that the imaginary interference caused by them was counteracted.

In OFDM systems, usually only one training symbol is used to generate a synchronization sequence, and this training symbol, e.g., the primary synchronization signal (PSS) in LTE, can also be used for channel estimation [24]. For the FBMC-OQAM, using only one symbol to perform the joint synchronization and channel estimation is difficult, owing to the issues mentioned above. The synchronization sequence and pilot sequence are usually designed separately [25], which will cause a large bandwidth efficiency loss. Joint synchronization and channel estimation schemes in the frequency domain have also been proposed [26]–[28]; however, no symbol TO [26] or only a fractional TO [27], [28] was assumed.

Inspired by these works, in this paper, we aim to present a novel FBMC-OQAM training sequence pattern that can perform joint symbol timing and channel estimation with a high bandwidth efficiency. Although the proposed training sequence is applicable to both burst and continuous transmission cases, it may be more suitable for the uplink of LTE-like systems, where the uplink signal is transmitted in burst mode and the CFO is compensated by downlink synchronization [29]. A pulse tail truncation scheme for the training sequence for the burst mode is also investigated to improve the bandwidth efficiency.

The remainder of this paper is organized as follows. Section II is devoted to describing the baseband system model of the FBMC-OQAM signal. The polyphase network system is described in matrix form. The scheme to generate a time synchronization sequence with CS property and a pulse tail truncation method for burst-mode transmissions are given in Section III. The symbol timing algorithm and channel estimation issue is addressed in Section IV. Some simulation results and discussions for a validation of the approach are presented in Section V. Finally, the conclusions are drawn in Section VI.

The following notations are used in this paper, $\mathrm{j} \triangleq \sqrt{-1}$, $|\cdot|$ denotes an absolute value, $\Re\{\cdot\}$ denotes a real part, and $\mathbb{E}[\cdot]$ the expectation. The superscripts $(\cdot)^*$, $(\cdot)^{\mathsf{T}}$, and $(\cdot)^{\mathsf{H}}$ represent the conjugate, transpose, and Hermitian conjugate operations, respectively. Bold lowercase letters denote column vectors, bold uppercase are used for matrices, $[\mathbf{X}]_{m,n}$ denotes the (m, n)-th entry of the matrix $\mathbf{X}$, $\mathrm{tr}(\mathbf{X})$ denotes the trace of $\mathbf{X}$, $\mathrm{diag}(\mathbf{x})$ denotes the diagonal matrix whose diagonal entries are the components of the vector $\mathbf{x}$, and $\mathbf{1}_{m,n}$ means an $m \times n$ matrix with all its elements being 1. In addition, $\otimes$ and $\circ$ denote the Kroneker product and Hadamard product, respectively, $\|\cdot\|$ denotes the Frobenius norm, and $\mathrm{vec}(\cdot)$ denotes the vectorization operator.

II. SYSTEM MODEL

A. BASEBAND MODEL OF FBMC-OQAM SYSTEMS

The basic idea of OQAM modulation is to separate the real and imaginary parts of a QAM symbol and stagger them by half of the QAM symbol period with a phase rotation. Namely, it can be considered that the modulated data symbols are real, i.e. PAM symbols, and the symbol period is half of that of QAM symbols to achieve the same bandwidth efficiency [1], [5].

Considering an FBMC-OQAM system with even number subcarriers M and let $x_{m,n}$ denote the real data transmitted by the m-th subcarrier and the n-th symbol, the transmitted

baseband signal $s(t)$ can be expressed as

$$s(t) = \sum_{n} \sum_{m=0}^{M-1} x_{m,n} \underbrace{\mathrm{j}^{m+n} \mathrm{e}^{\mathrm{j}2\pi mFt} p(t - nT)}_{p_{m,n}(t)}, \tag{1}$$

where j^{m+n} is the phase shift required to fulfill the real orthogonality condition for OQAM modulation, $p(t)$ denotes the prototype filter, which is usually a real symmetric filter with good TFL (e.g., PHYDYAS [30], IOTA [31] and Hermite [32] filters), and T and F, which satisfy $TF = 1/2$, are the symbol period and subcarrier bandwidth, respectively. The addends in (1) can be viewed as the data symbol $x_{m,n}$ passing a synthesis filter $p_{m,n}(t)$ in each subchannel.

Considering a multipath fading channel with the impulse response denoted by $h(\tau, t)$, the received signal can be represented as

$$r(t) = \int h(\tau, t) s(t - \tau)\, \mathrm{d}\tau + \omega(t), \tag{2}$$

where $\omega(t) \backsim \mathcal{CN}(0, P_\omega)$ denotes additive white Gaussian noise (AWGN).

By performing filtering to the received signal $r(t)$ at the receiver, we can obtain the (m, n)-th filtered signal $y_{m,n}$:

$$\begin{aligned} y_{m,n} &= \int r(t) q_{m,n}(t)\, \mathrm{d}t \\ &= x_{m,n} H_{m,n}^{0,0} + \sum_{(m',n') \neq (m,n)} x_{m',n'} H_{m,n}^{m'-m,n'-n} + \omega'_{m,n}, \end{aligned} \tag{3}$$

where $q_{m,n}(t)$ denotes the corresponding analysis filter, $\omega'_{m,n}$ is the effective noise after filtering, and $H_{m,n}^{m'-m,n'-n}$ represents the effective channel coefficient [8], [33] given by

$$H_{m,n}^{m'-m,n'-n} = \int\int h(\tau, t) p_{m',n'}(t - \tau) q_{m,n}(t)\, \mathrm{d}\tau\, \mathrm{d}t. \tag{4}$$

Even if the channel is ideal, the received symbol $y_{m,n}$ still suffers the imaginary intrinsic interference from the surrounding data points, and then $H_{m,n}^{m'-m,n'-n} = \mathrm{j}u_{m,n}^{m',n'}$, where the intrinsic interference weight $\mathrm{j}u_{m,n}^{m',n'}$ can be obtained as follows:

$$\mathrm{j}u_{m,n}^{m',n'} = \int p_{m',n'}(t) q_{m,n}(t)\, \mathrm{d}t. \tag{5}$$

Owing to the intrinsic interference, the channel coefficient $H_{m,n}^{0,0}$ cannot be estimated directly by transmitting a pilot at the (m, n)-th position. Nevertheless, if $H_{m,n}^{0,0}$ is known, we can obtain the received decision statistic $x'_{m,n}$ by performing the single-tap equalization and taking the real part of equalized signal to cancel the intrinsic interference, as follows:

$$x'_{m,n} = \Re\left\{ \frac{y_{m,n}}{H_{m,n}^{0,0}} \right\}. \tag{6}$$

B. MATRIX FORM OF THE BASEBAND TRANSMITTED SIGNAL

Let T_s denote the signal sampling period with the sampling rate $1/T_\mathrm{s} = MF$, and the discrete time version of $s(t)$ is given by

$$\begin{aligned} s(k) &\triangleq s(kT_\mathrm{s}) \\ &= \sum_{n} \sum_{m=0}^{M-1} x_{m,n} p_{m,n}(kT_\mathrm{s}) \qquad (7) \\ &= \sum_{n} \underbrace{\underbrace{\sum_{m=0}^{M-1} \left(\mathrm{j}^{m+n} x_{m,n}\right) \mathrm{e}^{\mathrm{j}\frac{2\pi mk}{M}}}_{\text{IDFT sequence } b_n(k)} \underbrace{p\big((k - nM/2)T_\mathrm{s}\big)}_{\text{prototype filter}}}_{\text{the } n\text{-th FBMC symbol signal}}. \qquad (8) \end{aligned}$$

According to (8), $s(k)$ consists of a series of single FBMC symbol signals, and each FBMC symbol signal can be regarded as the multiplication result of the sequence $b_n(k)$ and the prototype filter $p(k)$. It can be easily found that $b_n(k)$ is the inverse discrete Fourier transform (IDFT) of the sequence $\mathrm{j}^{m+n} x_{m,n}$.

For convenience, we represent the baseband system in matrix form. To simplify the analysis, M is chosen as a power of two, which is usually greater than 4. Let $\mathbf{s}$ denote the vector of the transmitted signal $s(k)$ with a total of K_total samples for N symbols and $\mathbf{x} = [x_{0,0}, x_{1,0}, \ldots, x_{M-1,0}, x_{0,1}, \ldots, x_{M-1,N-1}]^\mathsf{T}$ denote the vectorized forms of the data symbols, namely

$$\mathbf{x} = \mathrm{vec}(\mathbf{X}), \tag{9}$$

where

$$\begin{aligned} \mathbf{X} &= [\mathbf{x}_0, \mathbf{x}_1, \ldots, \mathbf{x}_{N-1}] \\ &= \begin{pmatrix} x_{0,0} & x_{0,1} & \cdots & x_{0,N-1} \\ x_{1,0} & x_{1,1} & \cdots & x_{1,N-1} \\ \vdots & \vdots & \ddots & \vdots \\ x_{M-1,0} & x_{M-1,1} & \cdots & x_{M-1,N-1} \end{pmatrix}. \end{aligned} \tag{10}$$

denotes the data symbol matrix. Similarly, let $\mathbf{P} = [\mathbf{p}_{0,0}, \mathbf{p}_{1,0}, \ldots, \mathbf{p}_{M-1,0}, \mathbf{p}_{0,1}, \ldots, \mathbf{p}_{M-1,N-1}]$ denote the corresponding synthesis filter signal matrix where $\mathbf{p}_{m,n} = [p_{m,n}(0), p_{m,n}(1), \ldots, p_{m,n}(K_\mathrm{total} - 1)]^\mathsf{T}$ denotes the samples of signal $p_{m,n}(t)$ during the whole signal duration. Then, (7) can be rewritten as

$$\mathbf{s} = \mathbf{P}\mathbf{x}. \tag{11}$$

To further investigate the composition of the transmitted signal, we first focus on the single FBMC symbol signal contained in $\mathbf{s}$.

Let $\mathbf{x}_n$ and $\mathbf{a}_n$ denote the n-th input data sequence without and with the phase rotation, respectively, and $\mathbf{a}_n$ is given by

$$\mathbf{a}_n = \boldsymbol{\theta}_n \circ \mathbf{x}_n, \tag{12}$$

where

$$\boldsymbol{\theta}_n = \left[\mathrm{j}^{n+0}, \mathrm{j}^{n+1}, \ldots, \mathrm{j}^{n+M-1}\right]^\mathsf{T} \tag{13}$$

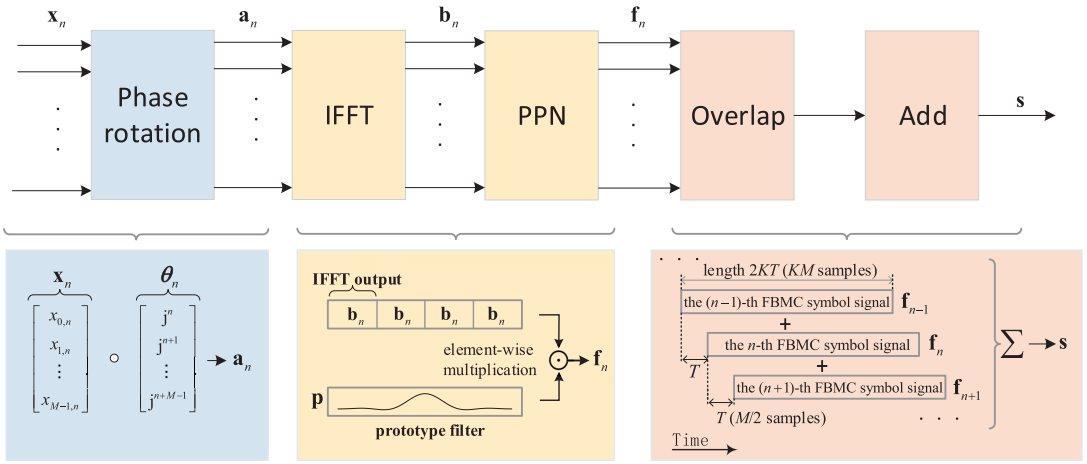

FIGURE 1. A conceptional point of view for FBMC-OQAM systems using a PPN.

denotes the phase factor added to $\mathbf{x}_n$. Then $\mathbf{b}_n$, the vector of $b_n(l)$ with $l = (k \mod M)$, is obtained by performing an IFFT of $\mathbf{a}_n$, namely

$$\mathbf{b}_n = \mathbf{F}_M^{\mathrm{H}} \mathbf{a}_n, \tag{14}$$

where $\mathbf{F}_M \in \mathbb{C}^{M\times M}$ denotes the discrete Fourier transform (DFT) matrix with the (l, m)-th element being $\mathrm{e}^{-\mathrm{j}2\pi lm/M}$.

Typically, the number of non-zero samples of the prototype filter is $KM - 1$, where K is the overlapping factor [34]. For simplicity, let the vector $\mathbf{p}$ with length KM denote the propotype filter signal by adding a zero sample $p(0)$ as the first sample. Similarly, let the vector $\mathbf{f}_n$ with length KM denote the valid samples of the n-th FBMC symbol signal. According to (8) and the fact that the IFFT sequence $b_n(k)$ is periodic, $\mathbf{f}_n$ can be calculated as

$$\mathbf{f}_n = (\mathbf{1}_{K\times 1} \otimes \mathbf{b}_n) \circ \mathbf{p}. \tag{15}$$

According to (15), the FBMC-OQAM transmitter can be implemented efficiently using the polyphase network (PPN) architecture [35], [36], which is shown in Fig. 1. The final transmitted signal $\mathbf{s}$ is a summation of $2K$ overlapped FBMC symbols with a time shift of $M/2$ samples. Considering that the lengths of $\mathbf{s}$ and $\mathbf{f}_n$ are $K_{total} = (N+2K-1)M/2$ and KM, respectively, if we divide $\mathbf{s}$ and $\mathbf{f}_n$ into sections with length $M/2$, namely,

$$\mathbf{s} = \left[\mathbf{s}_0^{\mathsf{T}}, \mathbf{s}_1^{\mathsf{T}}, \ldots, \mathbf{s}_{N+2K-1}^{\mathsf{T}}\right]^{\mathsf{T}}, \tag{16}$$

$$\mathbf{f}_n = \left[\mathbf{f}_{n,0}^{\mathsf{T}}, \mathbf{f}_{n,1}^{\mathsf{T}}, \ldots, \mathbf{f}_{n,2K-1}^{\mathsf{T}}\right]^{\mathsf{T}}. \tag{17}$$

then the n-th section of $\mathbf{s}$ can be represented by

$$\mathbf{s}_n = \sum_{i=0}^{2K-1} \mathbf{f}_{n-i,i}. \tag{18}$$

C. THE CONJUGATE SYMMETRY PROPERTY OF THE FBMC-OQAM SIGNAL

Because $\mathbf{x}_n$ is a real data sequence, a CS or conjugate antisymmetry property can be found for the IFFT output sequence $\mathbf{b}_n$. To be specific, $b_n(M/2 - l) = (-1)^n b_n^*(l)$ for $l = 0, 1, \ldots, M/2$, which can be derived as follows:

$$\begin{aligned} b_n(l) &= \mathrm{j}^n \sum_{m=0}^{M-1} \mathrm{j}^m x_{m,n} \mathrm{e}^{\mathrm{j}2\pi \frac{ml}{M}} \\ &= \mathrm{j}^n \sum_{m=0}^{M-1} x_{m,n} \mathrm{e}^{\mathrm{j}2\pi\left(\frac{m(l+M/4)}{M}\right)}, \end{aligned} \tag{19}$$

$$\begin{aligned} b_n\left(\frac{M}{2} - l\right) &= \mathrm{j}^n \sum_{m=0}^{M-1} x_{m,n} \mathrm{e}^{\mathrm{j}2\pi\left(\frac{m(M/2-l+M/4)}{M}\right)} \\ &= \mathrm{j}^n \sum_{m=0}^{M-1} x_{m,n} \mathrm{e}^{-\mathrm{j}2\pi\left(\frac{m(l+M/4)}{M}\right)} \\ &= (-1)^n b_n^*(l). \end{aligned} \tag{20}$$

Similarly, for $l = M/2+1, \ldots, 3M/4-1$, we obtain a similar relation:

$$b_n\left(\frac{3M}{2} - l\right) = (-1)^n b_n^*(l). \tag{21}$$

For simplicity, we treat both conjugate symmetry and conjugate antisymmetry as conjugate symmetry in this paper. Namely, $\mathbf{b}_n$ consists of two sequence sections that are conjugate symmetric. This CS property is shown in Fig. 2, and $\mathbf{b}_n$ can be divided into two half blocks, i.e.,

$$\mathbf{b}_n = \left[\mathbf{b}_{n,0}^{\mathsf{T}}, \mathbf{b}_{n,1}^{\mathsf{T}}\right]^{\mathsf{T}}. \tag{22}$$

Then, for $l = 1, 2, \ldots, M/2 - 1$, the following CS relationship is obtained:

$$b_{n,0}\left(\frac{M}{2} - l\right) = (-1)^n b_{n,0}^*(l), \tag{23}$$

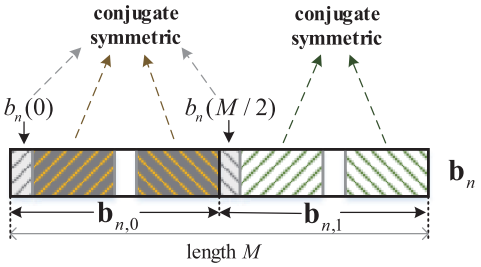

FIGURE 2. The conjugate symmetric pattern of the IFFT output sequence $\mathbf{b}_n$ with length M.

$$b_{n,1}\left(\frac{M}{2}-l\right)=(-1)^n b_{n,1}^*(l). \tag{24}$$

As in (17), if we also equally divide the prototype filter $\mathbf{p}$ into $2K$ sections, namely

$$\mathbf{p}=\left[\mathbf{p}_0^{\mathsf{T}},\mathbf{p}_1^{\mathsf{T}},\ldots,\mathbf{p}_{2K-1}^{\mathsf{T}}\right]^{\mathsf{T}}, \tag{25}$$

we can represent the i-th section $\mathbf{f}_{n,i}$ in (17) as

$$\mathbf{f}_{n,i}=\mathbf{b}_{n,(i \bmod 2)}\circ\mathbf{p}_i. \tag{26}$$

Although $\mathbf{b}_{n,(i \bmod 2)}$ is self-conjugate symmetric as in (23) and (24), it is easy to find that the exact CS property does not hold for $\mathbf{f}_{n,i}$, after element-wise multiplication with the asymmetric pulse shaping filter section $\mathbf{p}_i$ [15], [16]. Fig. 3 presents a view of the symmetric elements of $\mathbf{f}_n$ and $\mathbf{p}$. In addition to the pulse shaping effect, the symbol overlap as described in (18) further destroys the CS.

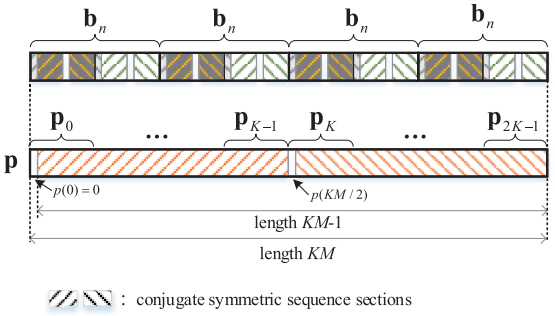

FIGURE 3. A view of the conjugate symmetric elements of the prototype filter $\mathbf{p}$ and repeated IFFT output sequence $\mathbf{b}_n$. The overlapping factor is 4.

III. TRAINING SEQUENCE WITH CS

A. THE METHOD FOR GENERATING A SEQUENCE WITH CS

As discussed in the previous subsection, the CS of the sequence $\mathbf{b}_n$ is destroyed by the pulse shaping and the symbol overlapping. In this section we introduce a method to generate a sequence with approximate CS property while maintaining a high bandwidth efficiency.

Fig. 4 shows the pulse shape of FBMC-OQAM symbols in the case of the Hermite filter, and we assume the sample values of $\mathbf{b}_n$ to be constant for clarity. Most of the energy

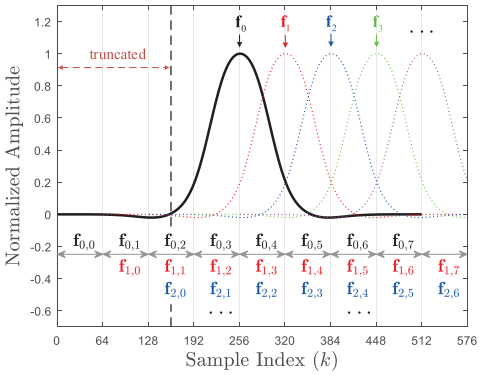

FIGURE 4. A view of the symbol overlap and a truncation scheme to shorten the pulse tails. The overlapping factor is 4.

of each FBMC symbol is concentrated in the several central sections, e.g., $\mathbf{f}_{K-1}$ and $\mathbf{f}_K$. Namely, only the immediately adjacent symbols significantly overlap with each other. In the following, we make an approximation to $\mathbf{s}_n$ by only considering three overlapped sections in (18). To be specific, $\mathbf{s}_{n+K}$, the $(n+K)$-th section of $\mathbf{s}$ is given by

$$\mathbf{s}_{n+K}\approx\mathbf{f}_{n,K}+\mathbf{f}_{n+1,K-1}+\mathbf{f}_{n+2,K-2} \tag{27}$$

or

$$\mathbf{s}_{n+K}\approx\mathbf{f}_{n,K}+\mathbf{f}_{n+1,K-1}+\mathbf{f}_{n-1,K+1}. \tag{28}$$

Given that filter $\mathbf{p}$ is symmetric, the mean power of $\mathbf{f}_{n+2,K-2}$ and $\mathbf{f}_{n-1,K+1}$ can be considered the same and thus (27) and (28) have the same approximation accuracy. To evaluate the approximation accuracy, we also define the approximation ratio $\gamma_{\text{appr},n}$, which is given by

$$\begin{aligned}\gamma_{\text{appr},n}&=\frac{\sum_{i=0,i\neq K-2,K-1,K}^{2K-1}\mathbb{E}\left[\|\mathbf{f}_{n+K-i,i}\|^2\right]}{\mathbb{E}\left[\|\mathbf{f}_{n,K}\|^2+\|\mathbf{f}_{n+1,K-1}\|^2+\|\mathbf{f}_{n+2,K-2}\|^2\right]}\\&=\frac{\sum_{i=0,i\neq K-1,K,K+1}^{2K-1}\mathbb{E}\left[\|\mathbf{f}_{n+K-i,i}\|^2\right]}{\mathbb{E}\left[\|\mathbf{f}_{n,K}\|^2+\|\mathbf{f}_{n+1,K-1}\|^2+\|\mathbf{f}_{n-1,K+1}\|^2\right]}.\end{aligned} \tag{29}$$

The mean values of $\gamma_{\text{appr},n}$ for different filters are shown in Table 1. In the case of burst-mode transmission, if $n=0$, there are no previous interference data symbols; thus, $\gamma_{\text{appr},0}$ is 3 dB better than that for $n\geqslant K-1$ during continuous transmission. The Hermite filter has the best time localization characteristics and thus the highest approximation ratio, and the PHYDYAS filter performs the worst. Although more signal sections can be considered to reduce the approximation error, it will be shown in Section V that the approximation in (27) and (28) introduces very limited performance loss to the symbol timing.

To exploit the conjugate symmetry property hidden in the FBMC-OQAM signal, we propose a preamble training sequence pattern as shown in Fig. 5. The first three symbols, a pilot symbol between two auxiliary data symbols, are used to generate the training sequence. The corresponding data

TABLE 1. The mean value of the approximation ratio $\gamma_{\text{appr},n}$ in dB for the hermite, PHYDYAS, and IOTA filters.

Transmission mode	$\gamma_{\text{appr},n}$		
	Hermite	PHYDYAS	IOTA
Burst ($n = 0$)	26.42	18.39	25.68
Continuous ($n \geqslant K-1$)	23.41	15.38	22.67

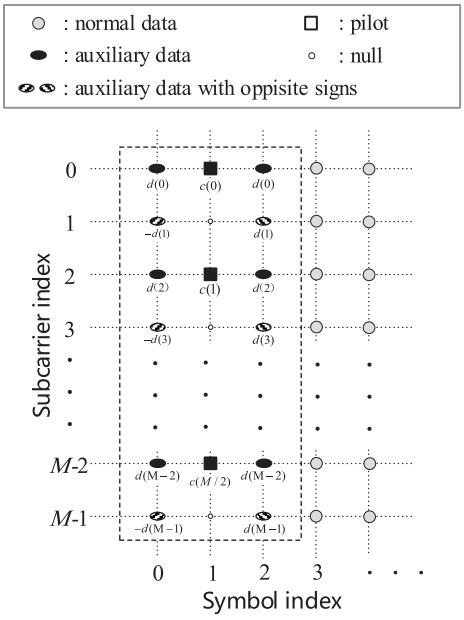

FIGURE 5. Frame structure of the proposed training sequence scheme in the time-frequency plane with *M* subcarriers.

sequences $\mathbf{x}_0$, $\mathbf{x}_1$, and $\mathbf{x}_2$ are given by

$$\begin{cases} x_{m,1} = c(m/2), & \text{for } m = 0, 2, \ldots, M-2; \\ x_{m,1} = 0, & \text{for } m = 1, 3, \ldots, M-1. \end{cases} \tag{30}$$

$$\begin{cases} x_{m,2} = x_{m,0} = d(m), & \text{for } m = 0, 2, \ldots, M-2; \\ x_{m,2} = -x_{m,0} = d(m), & \text{for } m = 1, 3, \ldots, M-1. \end{cases} \tag{31}$$

where $c(l)$ may denote a known pilot sequence used for the channel estimation discussed in next section, and $d(l)$ denotes an auxiliary data sequence. In the 1-st symbol, only even subcarriers are used for carrying data. The two auxiliary data symbols, namely $\mathbf{x}_0$ and $\mathbf{x}_2$, are the same, except that the data signs are opposite for the odd subcarriers. In fact, in (31), $\mathbf{x}_2$ can be regarded as a phase rotation of $\mathbf{x}_0$, as follows:

$$x_{m,2} = (-1)^m x_{m,0} = \mathrm{e}^{\mathrm{j}\pi m} x_{m,0}. \tag{32}$$

According to (30) and (32), the corresponding IDFT sequences $\mathbf{b}_1$ and $\mathbf{b}_2$ can be obtained by

$$\mathbf{b}_1 = \left[\mathbf{b}_{1,0}^{\mathsf{T}}, \mathbf{b}_{1,1}^{\mathsf{T}}\right]^{\mathsf{T}} = \left[\left(\mathbf{F}_{M/2}^{\mathsf{H}}\mathbf{c}\right)^{\mathsf{T}}, \left(\mathbf{F}_{M/2}^{\mathsf{H}}\mathbf{c}\right)^{\mathsf{T}}\right]^{\mathsf{T}}, \tag{33}$$

$$\mathbf{b}_2 = \left[\mathbf{b}_{2,0}^{\mathsf{T}}, \mathbf{b}_{2,1}^{\mathsf{T}}\right]^{\mathsf{T}} = \mathrm{j}^2 \cdot \left[\mathbf{b}_{0,1}^{\mathsf{T}}, \mathbf{b}_{0,0}^{\mathsf{T}}\right]^{\mathsf{T}} = \left[-\mathbf{b}_{0,1}^{\mathsf{T}}, -\mathbf{b}_{0,0}^{\mathsf{T}}\right]^{\mathsf{T}}, \tag{34}$$

where $\mathbf{c}$ denotes the sequence $c(k)$. As in (33) and (34), the two half parts of $\mathbf{b}_1$ are the same, and $\mathbf{b}_2$ is a $M/2$ point circular shift of $\mathbf{b}_0$. Then, according to (27) and (28), $\mathbf{s}_K$ and $\mathbf{s}_{K+1}$ are given by

$$\begin{aligned} \mathbf{s}_K &\approx \mathbf{f}_{0,K} + \mathbf{f}_{1,K-1} + \mathbf{f}_{2,K-2} \\ &= \mathbf{b}_{0,0} \circ \mathbf{p}_K + \mathbf{b}_{1,1} \circ \mathbf{p}_{K-1} + \mathbf{b}_{2,0} \circ \mathbf{p}_{K-2} \\ &= \underbrace{\mathbf{b}_{0,0} \circ \mathbf{p}_K}_{\text{item 1}} + \underbrace{\mathbf{b}_{1,0} \circ \mathbf{p}_{K-1}}_{\text{item 2}} + \underbrace{(-1) \cdot \mathbf{b}_{0,1} \circ \mathbf{p}_{K-2}}_{\text{item 3}}, \end{aligned} \tag{35}$$

$$\begin{aligned} \mathbf{s}_{K+1} &\approx \mathbf{f}_{2,K-1} + \mathbf{f}_{1,K} + \mathbf{f}_{0,K+1} \\ &= \mathbf{b}_{2,1} \circ \mathbf{p}_{K-1} + \mathbf{b}_{1,0} \circ \mathbf{p}_K + \mathbf{b}_{0,1} \circ \mathbf{p}_{K+1} \\ &= \underbrace{-\mathbf{b}_{0,0} \circ \mathbf{p}_{K-1}}_{\text{item 1}} + \underbrace{\mathbf{b}_{1,0} \circ \mathbf{p}_K}_{\text{item 2}} + \underbrace{\mathbf{b}_{0,1} \circ \mathbf{p}_{K+1}}_{\text{item 3}}. \end{aligned} \tag{36}$$

Considering the CS property of $\mathbf{b}_{0,0}$ and $\mathbf{p}$, we can find that items 1-3 in (35) are conjugate symmetric to those in (36); thus, $\mathbf{s}_K$ is conjugate symmetric to $\mathbf{s}_{K+1}$ as follows:

$$s_{K+1}\left(\frac{M}{2} - l\right) = -s_K^*(l), \quad \text{for } l = 1, 2, \ldots, \frac{M}{2} - 1. \tag{37}$$

The derivation details of (37) are given in (38), as shown at the bottom of this page. The signal composition and the CS relationship of $\mathbf{s}_K$ and $\mathbf{s}_{K+1}$ can also be observed in Fig. 6.

In addition, the proposed training sequence can also be applied to continuous-mode transmission. In this case, we assume that the pilot symbol is indexed by n and that the two auxiliary data symbols are indexed by $n-1$ and $n+1$. Then, the conjugate symmetric sequence sections are $\mathbf{s}_{n+K-1}$ and $\mathbf{s}_{n+K}$, and the following relationship can be similarly derived:

$$s_{n+K}\left(\frac{M}{2} - l\right) = (-1)^n s_{n+K-1}^*(l), \text{ for } l = 1, 2, \ldots, \frac{M}{2} - 1. \tag{39}$$

B. TRUNCATION OF THE TRAINING SEQUENCE

For burst-mode transmission, the long pulse tail, as shown in Fig. 4, may cause a bandwidth efficiency loss and additional latency [37]. In the multiuser uplink transmission of

$$\begin{aligned} s_{K+1}(M/2-l) &= -b_{0,0}(M/2-l)\,p_{K-1}(M/2-l) + b_{1,0}(M/2-l)\,p_K(M/2-l) + b_{0,1}(M/2-l)\,p_{K+1}(M/2-l) \\ &= -b_{0,0}^*(l)p_{K-1}(M/2-l) - b_{1,0}^*(l)p_K(M/2-l) + b_{0,1}^*(l)\,p_{K+1}(M/2-l) \\ &= -b_{0,0}^*(l)p_K(l) - b_{1,0}^*(l)p_{K-1}(l) + b_{0,1}^*(l)\,p_{K-2}(l) \\ &= -s_K^*(l) \qquad \text{for } l = 1, 2, \ldots, M/2-1 \end{aligned} \tag{38}$$

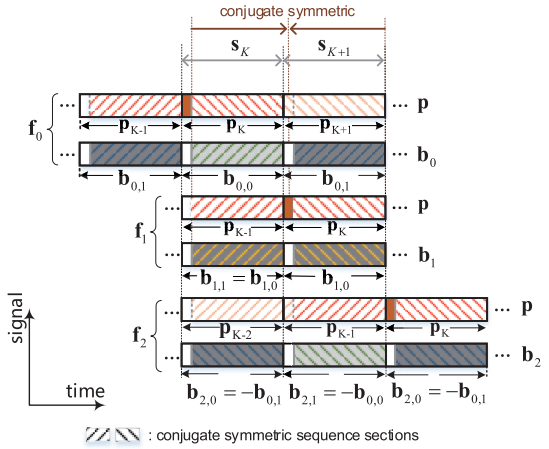

FIGURE 6. Time domain signal structure of the proposed training sequence and a CS property is hold between the K-th and $(K+1)$-th sections of the transmitted signal.

LTE-like systems, different users experience different phase rotations; thus, a long guard time is needed [37], [38]. To overcome this problem, several schemes including circulation filtering [39], [40], virtual symbols [37], and direct truncation [17], [41] have been proposed. In this paper, we propose a truncation scheme to improve the bandwidth efficiency.

As shown in Fig. 4, the signal during the first $2.5T$, i.e., $\mathbf{f}_{0,0}$, $\mathbf{f}_{0,1}$, and the first half part of $\mathbf{f}_{0,2}$, is considered to be truncated. To evaluate the effect of this truncation, we investigate the signal-to-interference ratio (SIR) of the truncated symbols in the following.

Like the synthesis filter matrix $\mathbf{P}$ in (11), let $\mathbf{Q} = [\mathbf{q}_{0,0}, \mathbf{q}_{1,0}, \ldots, \mathbf{q}_{M-1,0}, \mathbf{q}_{0,1}, \ldots, \mathbf{q}_{M-1,N-1}]$ denote the analysis filter signal matrix. Ignoring the channel and the noise, we can obtain the (m, n)-th received symbol as

$$y_{m,n} = \mathbf{q}_{m,n}^{\mathsf{T}}\mathbf{s} = \mathbf{q}_{m,n}^{\mathsf{T}}\mathbf{P}\mathbf{x}. \tag{40}$$

If there is a truncation, the corresponding samples in $\mathbf{P}$ are set to zero. After taking the real part of received symbols, the effective power of $y_{m,n}$ can be calculated as

$$\left|\Re\{y_{m,n}\}\right|^2 = \mathbf{x}^{\mathsf{T}}\mathbf{\Gamma}\mathbf{x}, \tag{41}$$

where

$$\mathbf{\Gamma} = \Re\left\{\mathbf{P}^{\mathsf{T}}\mathbf{q}_{m,n}\right\}\Re\left\{\mathbf{q}_{m,n}^{\mathsf{T}}\mathbf{P}\right\}. \tag{42}$$

If the data symbols are uncorrelated and have unit power, the mean SIR of the i-th symbol of $\mathbf{x}$ can be calculated as

$$\mathrm{SIR}_i = \frac{[\mathbf{\Gamma}]_{i,i}}{\mathrm{tr}\{\mathbf{\Gamma}\} - [\mathbf{\Gamma}]_{i,i}}. \tag{43}$$

According to (43), the mean SIRs among all the subcarriers of the first 3 truncated symbols are shown in Table 2. Because the energy of the truncated signal part is very low, the SIRs remain very high. Thus, it can be considered that the truncation has a negligible effect on the signal orthogonality.

TABLE 2. Mean SIRs of the truncated symbols for different filters.

Symbol	Signal-to-interference ratio (dB)		
	Hermite	PHYDYAS	IOTA
The 0th symbol	78.38	51.76	62.92
The 1st symbol	90.75	59.22	63.13
The 2nd symbol	104.65	66.45	63.21

TABLE 3. The number of required symbols for different training sequences with overlapping factor K. The symbol period is half of the QAM symbol period.

Method	Number of training symbols	Pulse-tail length (symbol period)	Total number of symbols
Proposed	2	0.5	2.5
[18]	4	K-1	K+3
[16]	4	0	4
[12]	K+4	K-1	$2K$+3

Considering that the truncation point is near a zero crossing of the filter signal, the truncated signal is supposed to maintain relatively low OOB radiation. The truncation effects on the bit error probability (BEP) and OOB are shown and discussed in Section V.

IV. SYMBOL TIMING AND CHANNEL ESTIMATION USING THE TRAINING SEQUENCE

A. SYMBOL TIMING ALGORITHM

Considering the CS relationship in (37), an auto-correlation-based TO estimation algorithm can be used for the symbol timing [42]. Let $r(k)$ denote the received baseband signal. The timing metric can be expressed as

$$W(l) = \frac{|V(l)|}{U(l)}, \tag{44}$$

where

$$V(l) = \sum_{\Delta l=1}^{M/2-1} 2r\big(l+\Delta l\big)r\big(l-\Delta l\big), \tag{45}$$

$$U(l) = \sum_{\Delta l=1}^{M/2-1} \left|r\big(l+\Delta l\big)\right|^2 + \left|r\big(l-\Delta l\big)\right|^2. \tag{46}$$

Owing to the CS property of the training sequence, $W(l)$ has a peak value at the correct sample index, while the values are trivial at all other positions. Thus, the correct sample index ϵ can be estimated from

$$\hat{\epsilon} = \arg\max_{l} W(l). \tag{47}$$

Because at least one payload data symbol can be transmitted via the two auxiliary data symbols, the actual number of additional symbols needed for training is 2. Thus, the bandwidth efficiency loss of the proposed training sequence is very limited, especially after the truncation. For burst-mode transmission, the number of required training symbols for several existing synchronization sequences and the proposed scheme is summarized in Table 3.

B. FREQUENCY DOMAIN CHANNEL ESTIMATION

As described in Section II, the received signal suffers from intrinsic interference. Thus, the channel estimation cannot be performed straightforwardly in FBMC-OQAM systems. Nevertheless, we will show that the pilots in the proposed training sequence can be used for channel estimation directly. This is because the intrinsic interference caused by the symbols surrounding the pilots cancels, which is similar to the preamble-based channel estimation method in [19].

Given that the prototype filter is well localized in both the time and frequency domains, the pilot is interfered by only nearby data points [23], [43], [44]. Considering that a pilot is transmitted at the (m, n)-th position in the time-frequency plane, Fig. 7 shows the values of the intrinsic interference weights $\mathrm{j}u_{m,n}^{m',n'}$ in (5) for the case of the Hermite filter.

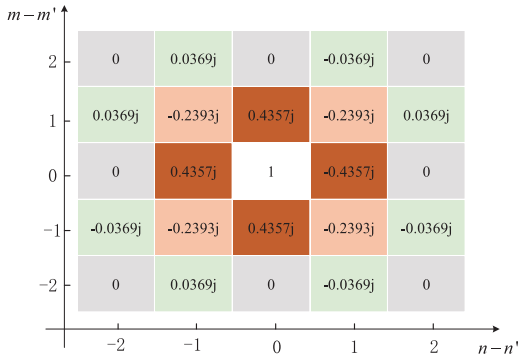

FIGURE 7. Imaginary interference $\mathrm{j}u_{m,n}^{m',n'}$ in the FBMC-OQAM using the Hermite filter with an overlapping factor of 4.

As shown in Fig. 7, the intrinsic interference is mainly caused by several adjacent data symbols. Usually, the nearest 8 data points are considered [23], [43], and we denote this neighborhood as $\Omega_{m,n}$, i.e., $0 < m'-m \leq 1$ and $0 < n'-n \leq 1$. In most cases, the interference caused by the data points out of $\Omega_{m,n}$ is negligible compared with the noise. In addition, the channel can be supposed to be flat with respect to $\Omega_{m,n}$ with a small size [23]. Accordingly, the received signal $y_{m,n}$ can be expressed as follows [23], [44]:

$$y_{m,n} \approx H_{m,n}^{0,0}\left(x_{m,n} + \mathrm{j}v_{m,n}\right) + \omega'_{m,n}, \tag{48}$$

where $\mathrm{j}v_{m,n}$ denotes the intrinsic interference from the data points in $\Omega_{m,n}$ and is given by

$$\mathrm{j}v_{m,n} = \textstyle\sum_{(m',n')\in\Omega} x_{m',n'}\mathrm{j}u_{m,n}^{m',n'}. \tag{49}$$

Under the effect of the phase factor j^{m+n} in (1), a specific symmetry pattern of $\mathrm{j}u_{m,n}$, as shown in Fig. 7, can be observed as follows [21]:

$$\begin{cases} u_{m,n}^{m+\Delta m,n+1} = -u_{m,n}^{m+\Delta m,n-1}, & \text{for } \Delta m = 0, 2, \ldots, M-2; \\ u_{m,n}^{m+\Delta m,n+1} = u_{m,n}^{m+\Delta m,n-1}, & \text{for } \Delta m = 1, 3, \ldots, M-1; \\ u_{m,n}^{m+\Delta m,n} = 0, & \text{for } \Delta m = 2, 4, \ldots, M-2. \end{cases} \tag{50}$$

Comparing the above symmetry pattern with the training sequence pattern in (30) and (31), we can easily find that for each pilot $c(l)$, the intrinsic interference from the adjacent auxiliary data points is canceled with each other. This process can be justified in the following equation:

$$\begin{aligned} \mathrm{j}v_{m,1} &= \sum_{0<\Delta n\leqslant 1, 0<\Delta m\leqslant 1} x_{m+\Delta m,n+\Delta n}\mathrm{j}u_{m,n}^{m+\Delta m,n+\Delta n} \\ &= \mathrm{j}\Big(d(m)\big(u_{m,1}^{m,0} + u_{m,1}^{m,2}\big) + d(m+1)\big(u_{m,1}^{m+1,2} \\ &\quad - u_{m,1}^{m+1,0}\big) + d(m-1)\big(u_{m,1}^{m-1,2} - u_{m,1}^{m-1,0}\big)\Big) \\ &= 0 \qquad \text{for } m = 0, 2, \ldots, M-2. \end{aligned} \tag{51}$$

According to (48), the channel coefficient at the m-th subcarrier in the 1-st symbol can thus be estimated by

$$\hat{H}_{m,1}^{0,0} = \frac{y_{m,1}}{c(m/2)} \quad \text{for } m = 0, 2, \ldots, M-2. \tag{52}$$

Note that not all the even subcarriers in the 1-st symbol should be occupied by pilots. If the frequency selectivity of the channel is not severe, a part of the even subcarriers can be used for payload data to further improve the bandwidth efficiency.

V. NUMERICAL SIMULATION RESULTS

In this section, the proposed scheme is validated via simulations. The symbol timing accuracy is evaluated by the root mean square error (RMSE) defined as $\left(\mathbb{E}[(\hat{\epsilon}-\epsilon)^2]\right)^{1/2}$. The BEPs for the cases of the estimated channel and perfect channel are compared. Both the RMSE and the BEP are functions of the signal-to-noise ratio (SNR). The SNR for the FBMC-OQAM is defined as $\mathbb{E}\left[|x_{m,n}|^2\right]/(P_\omega/2)$ [4]. In the simulation, 1×10^4 Monter Carlo trials are performed with the following conditions:

1) The subcarrier bandwidth is set as $F = 15$ kHz, the number of subcarriers M is 256, and the sampling rate is 15.36 MHz.
2) The payload data symbols are the real and imaginary parts of 4QAM or 16-QAM data symbols.
3) The Hermite filter with an overlapping factor of $K = 4$ is considered as the prototype filter, and the exceptions are specified.
4) Three channel models, including AWGN and two multipath channels, ITU Pedestrian A (Ped-A) at 3 km/hour and Vehicular A (Veh-A) at 60 km/hour [45], are considered.
5) The number of FBMC symbols is 10. The symbols indexed by the 0 to 2 are used to generate the proposed training sequence, and the 3rd symbol is used for the BEP calculation. Six symbol intervals of pure noise are included at the beginning of the transmitted signal.
6) The number of pilots is 64; i.e., half of the even subcarriers of the 1st symbol are used to carry pilots, and the rest are used for payload data. The pilot sequence $c(m)$ is chosen as a pseudo-noise sequence. Because the odd subcarriers are null, all the data in the 1st symbol are multiplied by a power boost factor of 2 so that all the FBMC symbols have the same power.

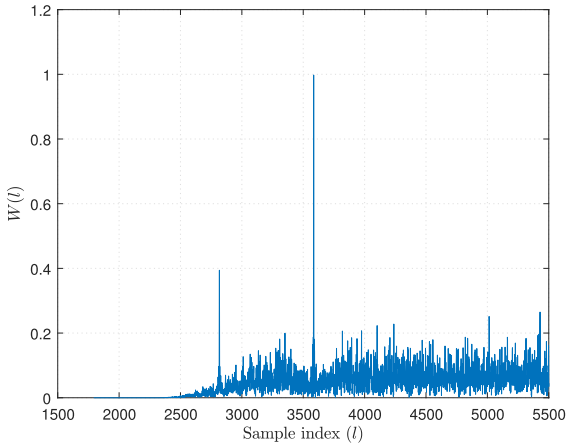

FIGURE 8. A typical realization of the timing metric $W(l)$ in (44) without noise.

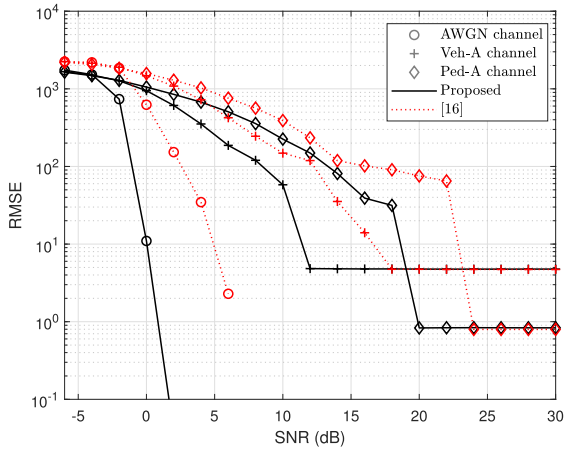

FIGURE 9. RMSEs of the symbol timing over three channels: AWGN, ITU Pedestrian-A, and ITU Vehicular-A. The payload data are based on 4QAM symbols.

Fig. 8 shows a realization of the timing metric $W(l)$ ignoring the channel distortion and noise. A main peak point that denotes the right time index and a side peak point can be observed. The side peak point is caused by a part of the starting signal that also preserves an approximated CS property [15]. However, the amplitude of the side peak point is much lower than the main peak point, and the number of peak points is much less than that for the methods in [16], [18]. Thus, better symbol timing is supposed for the proposed method.

Fig. 9 shows the RMSEs of the proposed TO estimator. Because in [18] the authors showed that the method proposed in [16] has the best symbol timing RMSE compared with that in [12], [18], its performance is also presented as a comparison. In Fig. 9, it can be found that the proposed method is superior to the method in [16] in all three channels. The timing performance in the AWGN channel is much better than that in the multipath channels. In the high-SNR region, both methods show timing error floors in the Veh-A and Ped-A channels. This is because that there are multiple delay taps in these channels and the strongest tap is not always the first

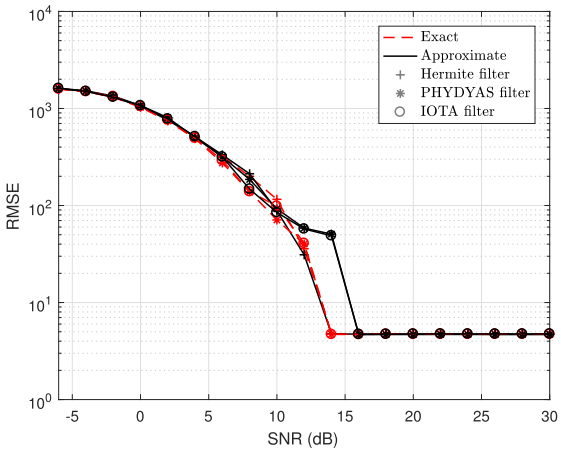

FIGURE 10. RMSEs of the symbol timing for a continuous-mode transmission over the ITU Vehicular-A channel. The training sequences with approximate and exact CS properties are both considered and compared in the case of three prototype filters: Hermite, PHYDYAS, and IOTA. The payload data are based on 16QAM symbols.

one, which we treat as the right timing baseline, owing to the Rayleigh fading process, and the dectection error exists even without the noise. The error floor is higher in the Veh-A channel owing to the longer mean delay spread compared with the Ped-A channel. However, in the low-SNR region, the performance in the Veh-A channel is better than that in the Ped-A channel. This is because there are several strong delay taps in the Veh-A channel, and the probability that all taps are in deep fade is lower than that in the Ped-A channel; thus, the RMSE is smaller.

As discussed in Section III, the proposed training sequence is conjugate symmetric when the approximation in (27) and (28) is made, and the approximation error is lager in continuous-mode transmission. Fig. 10 shows the RMSE of the proposed scheme in continuous-mode transmission where the training sequence is placed in the middle of the transmitted signal. A higher modulation type, 16QAM, is used for payload data symbols including the auxiliary symbols. In addition, the symbol timing performance of an exact conjugate symmetric sequence that is generated by $2K$ auxiliary symbols according to (31) is also presented. We can observe that the proposed approximation method shows a negligible effect on the symbol timing performance when the Hermite filter is used. Similar results can also be observed for the PHYDYAS and IOTA filters for most SNR values.

The truncation effect on the BEP of the truncated symbols is described in Fig. 11. The 0th and 2nd symbols, namely the auxiliary data symbols, are considered. As discussed in Section III, the BEP of the 0th symbol using the PHYDYAS filter degrades the most owing to the lowest SIR. The BEP of the 2nd symbols is slightly better than that of the 0th symbol, which is consistent with the data in Table 2. Nevertheless, the BEP performance loss of all the truncated symbols is very limited. On one hand, this is due to that the SIRs of the truncated symbols are relatively high. On the other hand,

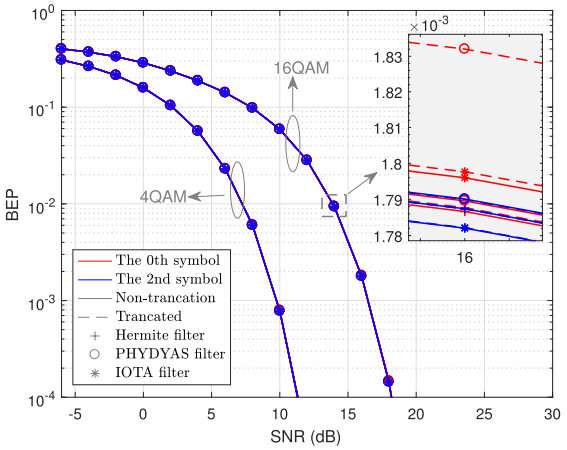

FIGURE 11. BEP performance of the 0th and 2nd symbols with and without the truncation for different filter cases.

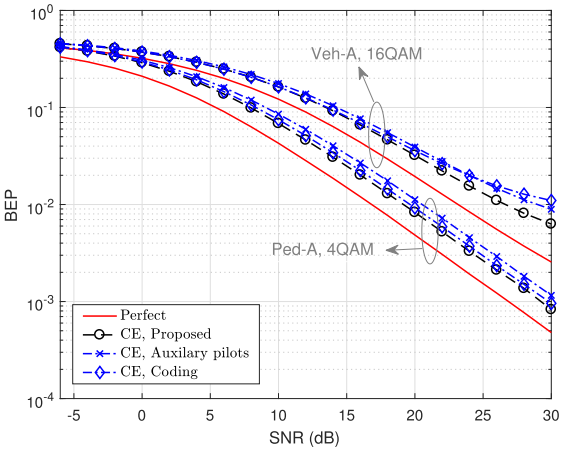

FIGURE 13. BEP of the channel estimation (CE) methods in the Pedestrian A and Vehicular A channels.

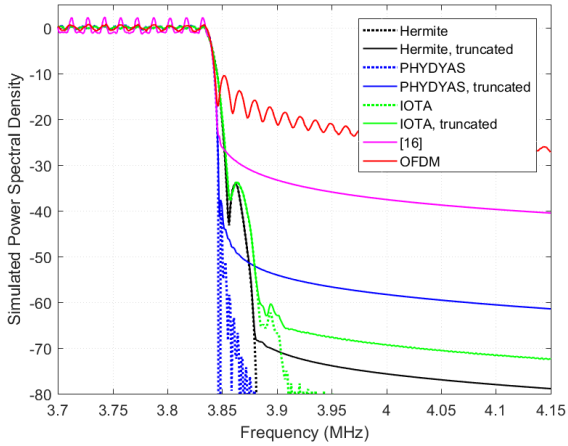

FIGURE 12. Power spectrum density of the transmitted signal with and without the truncation. The signal bandwidth is 3.84 MHz with a 15KHz subcarrier spacing.

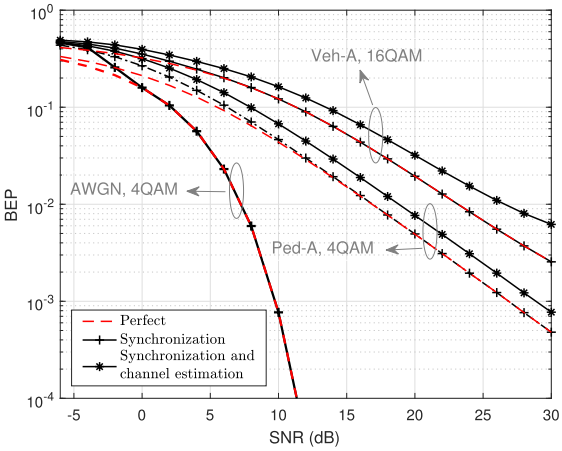

FIGURE 14. BEP of the proposed time synchronization and channel estimation methods.

the noise power is possibly higher than the truncated part of the signal because the power of the truncated part is very low; thus, the truncation also helps to reduce the noise power when the SNR is not very high.

The OOB radiation of the truncated signal is relatively low, as shown in Fig. 12. If there is no truncation, the PHYDYAS filter has the lowest OOB radiation according to the signal power spectrum density (PSD) curves. In the case of the proposed truncation, however, the OOB radiation of the PHYDYAS filter is obviously increased. The truncation effect on the IOTA and Hermite filters are much smaller. That is because the time localization of the Hermite and IOTA filters is superior to that of the PHYDYAS filter. The Hermite filter with the truncation shows good OOB performance in terms of both a fast sidelobe decay and high stop-band attenuation. Because the truncation point is near a zero-crossing point, the proposed sequence shows much better OOB performance than that of the sequence scheme in [16] and the OFDM signal while maintaining a high bandwidth efficiency. In addition, we can observe that there is a larger in-band ripple for the training sequence in [16].

Fig. 13 shows the BEP for the channel estimation. As a comparison, the results of the AP [22] and the coding [23] channel estimation methods are also presented. The same pilot pattern is used for all methods, and the channel coefficients of the positions without pilots are obtained by linear interpolation. Considering the pilot density, the largest 8 interference signals from adjacent data points are canceled in the AP and the coding methods. We can observe that the BEP degradation caused by the channel estimation does not decrease as the SNR increases. The proposed method and the coding method perform slightly better than the AP method in the Ped-A channel, given that the AP method introduces a power penalty to payload data assuming the same transmitting power.. However, when the SNR is larger than 18 dB in the Veh-A channel, the performance of the coding method also deteriorates. This indicates that large inter symbol interference (ISI) and ICI will seriously affect the performance of the coding method.

The BEPs for the proposed symbol TO estimator are presented in Fig. 14. Compared with the time synchronization, the channel estimation degrades the BEP more distinctly. If the channel is perfectly known and only the proposed time synchronization scheme is considered, there is nearly no performance degradation over the AWGN channel when the SNR is larger than 0 dB, and the Veh-A channel is 6 dB. In the case of the Ped-A channel, owing to the slower rate of decrease in the syobol timing RMSE, as shown in Fig. 9, the BEP degradation exists for a larger SNR region.

VI. CONCLUSION

In this paper, a new training sequence pattern has been proposed for joint symbol timing and channel estimation in FBMC-OQAM systems. By exploiting the CS property of the training sequence, a symbol timing algorithm has been introduced. Meanwhile, the imaginary interference introduced to the pilots in the training sequence is canceled by symmetric auxiliary data points; thus, the channel coefficients can be estimated directly by the pilots. Because the auxiliary data symbols in the training sequence can also be used to transmit payload data, the proposed training sequence achieves a very high bandwidth efficiency. In particular, a pulse tail truncation scheme has also been proposed to further improve the bandwidth efficiency for burst-mode transmission. The SIRs of the truncated symbols have been analyzed and show a negligible effect on the signal orthogonality. The simulation results demonstrate that the proposed scheme achieves good performances in terms of timing accuracy, BEP, and OOB radiation and is applicable to both burst- and continuous-mode transmission.

REFERENCES

[1] B. Farhang-Boroujeny, "OFDM versus filter bank multicarrier," *IEEE Signal Process. Mag.*, vol. 28, no. 3, pp. 92–112, May 2011.

[2] C. Sexton, Q. Bodinier, A. Farhang, N. Marchetti, F. Bader, and L. A. DaSilva, "Enabling asynchronous machine-type D2D communication using multiple waveforms in 5G," *IEEE Internet Things J.*, vol. 5, no. 2, pp. 1307–1322, Apr. 2018.

[3] H. Zhang, D. Le Ruyet, D. Roviras, Y. Medjahdi, and H. Sun, "Spectral efficiency comparison of OFDM/FBMC for uplink cognitive radio networks," *EURASIP J. Adv. Signal Process.*, vol. 2010, Dec. 2010, Art. no. 621808.

[4] R. Nissel and M. Rupp, "OFDM and FBMC-OQAM in doubly-selective channels: Calculating the bit error probability," *IEEE Commun. Lett.*, vol. 21, no. 6, pp. 1297–1300, Jun. 2017.

[5] R. Nissel, S. Schwarz, and M. Rupp, "Filter bank multicarrier modulation schemes for future mobile communications," *IEEE J. Sel. Areas Commun.*, vol. 35, no. 8, pp. 1768–1782, Aug. 2017.

[6] A. Sahin, I. Guvenc, and H. Arslan, "A survey on multicarrier communications: Prototype filters, lattice structures, and implementation aspects," *IEEE Commun. Surveys Tuts.*, vol. 16, no. 3, pp. 1312–1338, 3rd Quart., 2014.

[7] P. Tan and N. C. Beaulieu, "Effect of channel estimation error on bit error probability in OFDM systems over Rayleigh and Ricean fading channels," *IEEE Trans. Commun.*, vol. 56, no. 4, pp. 675–685, Apr. 2008.

[8] L. Li, Y. Wang, and L. Ding, "On the bit error probability of OFDM and FBMC-OQAM systems in Rayleigh and Rician multipath fading channels," *IEICE Trans. Commun.*, vol. 102, no. 12, Dec. 2019. [Online]. Available: https://www.jstage.jst.go.jp/article/transcom/advpub/0/advpub_2017EBP3451/_article. doi: 10.1587/transcom.2017EBP3451.

[9] P. Ciblat and E. Serpedin, "A fine blind frequency offset estimator for OFDM/OQAM systems," *IEEE Trans. Signal Process.*, vol. 52, no. 1, pp. 291–296, Jan. 2004.

[10] T. Fusco and M. Tanda, "Blind frequency-offset estimation for OFDM/OQAM systems," *IEEE Trans. Signal Process.*, vol. 55, no. 5, pp. 1828–1838, May 2007.

[11] T. Fusco, A. Petrella, and M. Tanda, "Blind carrier-frequency offset estimation for pulse shaping OFDM/OQAM systems," in *Proc. 3rd Int. Symp. Commun., Control Signal Process.*, Mar. 2008, pp. 942–947.

[12] T. Fusco, A. Petrella, and M. Tanda, "Data-aided symbol timing and CFO synchronization for filter bank multicarrier systems," *IEEE Trans. Wireless Commun.*, vol. 8, no. 5, pp. 2705–2715, May 2009.

[13] W. Chung, C. Kim, S. Choi, and D. Hong, "Synchronization sequence design for FBMC/OQAM systems," *IEEE Trans. Wireless Commun.*, vol. 15, no. 10, pp. 7199–7211, Oct. 2016.

[14] L. Li, Y. Wang, and L. Ding, "Time synchronization sequence with weighted conjugate symmetry property for FBMC-OQAM systems," in *Proc. IEEE Mil. Commun. Conf. (MILCOM)*, Oct. 2018, pp. 1–6.

[15] D. Mattera and M. Tanda, "Blind symbol timing and CFO estimation for OFDM/OQAM systems," *IEEE Trans. Wireless Commun.*, vol. 12, no. 1, pp. 268–277, Jan. 2013.

[16] D. Mattera and M. Tanda, "Data-aided synchronization for OFDM/OQAM systems," *Signal Process.*, vol. 92, no. 9, pp. 2284–2292, Sep. 2012.

[17] M. Bellanger, "Efficiency of filter bank multicarrier techniques in burst radio transmission," in *Proc. IEEE GLOBECOM*, Dec. 2010, pp. 1–4.

[18] H. Cho and X. Ma, "Generalized synchronization algorithms for FBMC-OQAM systems," *IEEE Trans. Veh. Technol.*, vol. 67, no. 10, pp. 9764–9774, Oct. 2018.

[19] S. Hu, G. Wu, T. Li, Y. Xiao, and S. Li, "Preamble design with ICI cancellation for channel estimation in OFDM/OQAM system," *IEICE Trans. Commun.*, vols. E93–B, no. 1, pp. 211–214, Jan. 2010.

[20] C. Lele, P. Siohan, and R. Legouable, "2 dB better than CP-OFDM with OFDM/OQAM for preamble-based channel estimation," in *Proc. IEEE ICC*, May 2008, pp. 1302–1306.

[21] E. Kofidis, D. Katselis, A. Rontogiannis, and S. Theodoridis, "Preamble-based channel estimation in OFDM/OQAM systems: A review," *Signal Process.*, vol. 93, no. 7, pp. 2038–2054, 2013.

[22] J.-P. Javaudin, D. Lacroix, and A. Rouxel, "Pilot-aided channel estimation for OFDM/OQAM," in *Proc. IEEE Veh. Technol. Conf. (VTC)*, vol. 3. Sep. 2003, pp. 1581–1585.

[23] C. Lele, C. Lele, R. Legouable, and P. Siohan, "Channel estimation with scattered pilots in OFDM/OQAM," in *Proc. IEEE 9th Workshop Signal Process. Adv. Wireless Commun. (SPAWC)*, Jul. 2008, pp. 286–290.

[24] S. Sesia, M. Baker, and I. Toufik, "Synchronization and cell search," in *LTE—The UMTS Long Term Evolution: From Theory to Practice*, 2nd ed. London, U.K.: Wiley, 2011, pp. 153–161.

[25] Y. Zeng and M. W. Chia, "Joint time-frequency synchronization and channel estimation for FBMC," in *Proc. PIMRC*, Sep. 2014, pp. 438–442.

[26] P. Singh and K. Vasudevan, "Frequency synchronization and channel estimation for OFDM/OQAM signals transmitted through Rayleigh fading channels," in *Proc. 23rd Nat. Conf. Commun. (NCC)*, Mar. 2017, pp. 1–6.

[27] T. H. Stitz, T. Ihalainen, and M. Renfors, "Practical issues in frequency domain synchronization for filter bank based multicarrier transmission," in *Proc. 3rd Int. Symp. Commun., Control Signal Process. (ISCCSP)*, Mar. 2008, pp. 411–416.

[28] T. H. Stitz, T. Ihalainen, A. Viholainen, and M. Renfors, "Pilot-based synchronization and equalization in filter bank multicarrier communications," *EURASIP J. Adv. Signal Process.*, vol. 2010, no. 1, 2010, Art. no. 741429.

[29] L. Haring, S. Bieder, and A. Czylwik, "Fine frequency synchronization in the uplink of multiuser OFDM systems," *IEEE Trans. Commun.*, vol. 57, no. 12, pp. 3743–3752, Dec. 2009.

[30] S. Mirabbasi and K. Martin, "Overlapped complex-modulated transmultiplexer filters with simplified design and superior stopbands," *IEEE Trans. Circuits Syst. II, Analog Digit. Signal Process.*, vol. 50, no. 8, pp. 456–469, Aug. 2003.

[31] B. Le Floch, M. Alard, and C. Berrou, "Coded orthogonal frequency division multiplex," *Proc. IEEE*, vol. 83, no. 6, p. 982–996, Jun. 1995.

[32] R. Haas and J.-C. Belfiore, "A time-frequency well-localized pulse for multiple carrier transmission," *Wireless Pers. Commun.*, vol. 5, no. 1, pp. 1–18, Jan. 1997.

[33] M. Fuhrwerk, S. Moghaddamnia, and J. Peissig, "Scattered pilot-based channel estimation for channel adaptive FBMC-OQAM systems," *IEEE Trans. Wireless Commun.*, vol. 16, no. 3, pp. 1687–1702, Mar. 2017.

[34] A. Viholainen, T. Ihalainen, T. H. Stitz, M. Renfors, and M. Bellanger, "Prototype filter design for filter bank based multicarrier transmission," in *Proc. 17th Eur. Signal Process. Conf. (EUSIPCO)*, Aug. 2009, pp. 1359–1363.
[35] M. Bellanger *et al.*, *FBMC Physical Layer: A Primer*, PHYDYAS FP7 Project Document, Jan. 2010.
[36] D. Na and K. Choi, "Low PAPR FBMC," *IEEE Trans. Wireless Commun.*, vol. 17, no. 1, pp. 182–193, Jan. 2017.
[37] D. Qu, F. Wang, Y. Wang, T. Jiang, and B. Farhang-Boroujeny, "Improving spectral efficiency of FBMC-OQAM through virtual symbols," *IEEE Trans. Wireless Commun.*, vol. 16, no. 7, pp. 4204–4215, Jul. 2017.
[38] R. Nissel and M. Rupp, "Pruned DFT-spread FBMC: Low PAPR, low latency, high spectral efficiency," *IEEE Trans. Commun.*, vol. 66, no. 10, pp. 4811–4825, Oct. 2018.
[39] M. J. Abdoli, M. Jia, and J. Ma, "Weighted circularly convolved filtering in OFDM/OQAM," in *Proc. PIMRC*, Sep. 2013, pp. 657–661.
[40] A. Rezazadeh-Reyhani and B. Farhang-Boroujeny, "Capacity analysis of FBMC-OQAM systems," *IEEE Commun. Lett.*, vol. 21, no. 5, pp. 999–1002, May 2017.
[41] A. Zafar, L. Zhang, P. Xiao, and M. A. Imran, "Spectrum efficient MIMO-FBMC system using filter output truncation," *IEEE Trans. Veh. Technol.*, vol. 67, no. 3, pp. 2367–2381, Mar. 2018.
[42] B. Park, H. Cheon, C. Kang, and D. Hong, "A novel timing estimation method for OFDM systems," *IEEE Commun. Lett.*, vol. 7, no. 5, pp. 239–241, May 2003.
[43] W. Cui, D. Qu, T. Jiang, and B. Farhang-Boroujeny, "Coded auxiliary pilots for channel estimation in FBMC-OQAM systems," *IEEE Trans. Veh. Technol.*, vol. 65, no. 5, pp. 2936–2946, May 2016.
[44] J.-M. Choi, Y. Oh, H. Lee, and J.-S. Seo, "Pilot-aided channel estimation utilizing intrinsic interference for FBMC/OQAM systems," *IEEE Trans. Broadcast.*, vol. 63, no. 4, pp. 644–655, Dec. 2017.
[45] *Guidelines for Evaluation of Radio Transmission Technologies for IMT-2000*, ITU, Geneva, Switzerland, document ITU-R M.1225, 1997.

LIMING LI (S'16) received the B.E. degree in communication engineering from Shandong University, Jinan, China, in 2007, and the M.S. degree in biomedical engineering from Chongqing University, Chongqing, China, in 2013. He is currently pursuing the Ph.D. degree in information and communication engineering with the Harbin Institute of Technology, Shenzhen, China. His research interests include multicarrier modulation, synchronization, equalization, and digital signal processing.

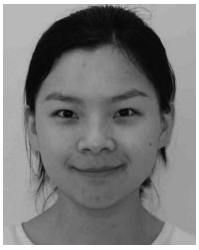

LIQIN DING (M'17) received the B.E., M.E., and Ph.D. degrees in information and communication engineering from the Harbin Institute of Technology, Harbin, China, in 2009, 2011, and 2017, respectively. She visited the Department of Electronics and Telecommunications, Norwegian University of Science and Technology, from September 2012 to September 2014, and the Department of Electronic and Electrical Engineering, The University of Sheffield, U.K., from August to December 2016. She is currently a Postdoctoral Fellow with the School of Electronic and Information Engineering, Harbin Institute of Technology at Shenzhen, Shenzhen, China. Her research interests include cellular-based vehicle-to-everything communication, ultra-dense networks, lattice-based MIMO detection, and cooperative communications.

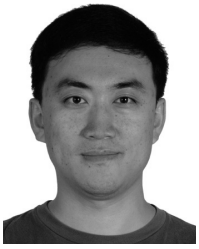

YANG WANG received the Ph.D. degree in communication and information system from the Harbin Institute of Technology, Harbin, China, in 2005, where he was a Postdoctoral Fellow with the Shenzhen Graduate School, from 2005 to 2007. He has been an Associate Professor with the School of Electronic and Information Engineering, Harbin Institute of Technology at Shenzhen, Shenzhen, China, since 2007. He is also a Senior Member of the Chinese Institute of Electronics. His research interests include a wide range of topics in wireless communications and signal processing, including vehicular communications, MIMO systems, MIMO channel measurement and modeling, cooperative communications, and underwater wireless charging and communication systems.

PENG WU (S'16) received the B.E. degree in information engineering from the Wuhan University of Technology, Wuhan, China, in 2015. He is currently pursuing the Ph.D. degree with the School of Electronic and Information Engineering, Harbin Institute of Technology at Shenzhen, Shenzhen, China. He visited the Department of Science and Technology, Linkoping University, Sweden, from June to September 2016, and the Department of Electronic and Electrical Engineering, The University of Sheffield, U.K., in February 2018. His research interests include vehicular communication networks and intelligent transportation systems.

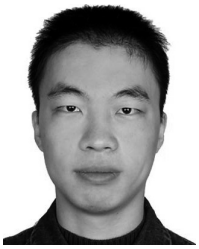

JILIANG ZHANG (M'14–SM'19) received the B.E., M.E., and Ph.D. degrees from the Harbin Institute of Technology, Harbin, China, in 2007, 2009, and 2014, respectively, where he was a Postdoctoral Fellow with the Shenzhen Graduate School, from 2014 to 2016, an Associate Professor with the School of Information Science and Engineering, Lanzhou University, in 2017, and a Researcher with the Department of Electrical Engineering, Chalmers University of Technology, Gothenburg, Sweden. He is currently a Marie Curie Research Fellow with the Department of Electronic and Electrical Engineering, The University of Sheffield, Sheffield, U.K. His research interests include a wide range of topics in wireless systems, in particular including MIMO channel measurement and modeling, single radio frequency MIMO system, relay system, and wireless ranging systems.